Supplemental Information

Periodic-shRNA Molecules are Capable of Gene Silencing, Cytotoxicity and Innate Immune Activation in Cancer Cells

Kevin E. Shopsowitz[1,2], Connie Wu[1,2], Gina Liu[1,2], Erik C. Dreaden[1,2], and Paula T. Hammond[1,2,3]*

[1] Koch Institute for Integrative Cancer Research, Massachusetts Institute of Technology, Cambridge, Massachusetts

[2]Department of Chemical Engineering, Massachusetts Institute of Technology, Cambridge, Massachusetts

[3]Institute for Soldier Nanotechnologies, Massachusetts Institute of Technology, Cambridge, Massachusetts

* To whom correspondence should be addressed. Tel:1-617-258-7577; Fax: 1-617-258-8992; Email: hammond@mit.edu

Table S1. DNA Template Sequences Used in this Study[i]

Code	Name	Sequence
1	GFP-3 (22 bp)	5'P-**CCTGAAGTTCAT**GAC**ATGAACTTCAGGGTCAGCTTGCT**GAC**AGCAAGCTGAC**
2	GFP-5 (21 bp)	5'P-**CCTGAAGTTCA**TTGTT**TGAACTTCAGGGTCAGCTTGC**TTGTT**GCAAGCTGAC**
3	GFP-6 (22 bp)	5'P-**CCTGAAGTTCAT**GACAGG**ATGAACTTCAGGGTCAGCTTGCT**GACAGG**AGCAAGCTGAC**
4	GFP-8 (21 bp)	5'P-**CCTGAAGTTCA** ACAGGAAG**TGAACTTCAGGGTCAGCTTGC**ACAGGAAG**GCAAGCTGAC**
5	GFP-5/10 (21 bp)	5'P-**CCTGAAGTTCA**TGACAGGAAG**TGAACTTCAGGGTCAGCTTGC**TTGTT**GCAAGCTGAC**
6	GFP-10a (21 bp)	5'P-**CCTGAAGTTCA**TGACAGGAAG**TGAACTTCAGGGTCAGCTTGC** TGACAGGAAG**GCAAGCTGAC**
7	GFP-10b (21 bp)	5'P-**CCTGAAGTTCA**TGACAGGAAG**TGAACTTCAGGGTCAGCTTGC** TGAGAGGAAG**GCAAGCTGAC**
8	GFP-10c (21 bp)	5'P-**CCTGAAGTTCA**TGAGAGGAAG**TGAACTTCAGGGTCAGCTTGC** TGAGAGGAAG**GCAAGCTGAC**
9	GFP-10d (21 bp)	5'P-**CCTGAAGTTCA**TCCGACCAGC**TGAACTTCAGGGTCAGCTTGC** TCCGACCAGC**GCAAGCTGAC**
10	GFP-10e (21 bp)	5'P-**CCTGAAGTTCA**CCCCCCCCCC**TGAACTTCAGGGTCAGCTTGC** CCCCCCCCCC**GCAAGCTGAC**
11	GFP-12 (21 bp)	5'P-**CCTGAAGTTCA**TGACAGGAAGAT**TGAACTTCAGGGTCAGCTTGC**TGACAGGAAGAT **GCAAGCTGAC**
12	GFP-10 (25 bp)	5'P- **CCTGAAGTTCATCTG**TGACAGGAAG**CAGATGAACTTCAGGGTCAGCTTGC**TGACAGGAAG **GCAAGCTGAC**
13	GFP-10 (25 bp w/ mismatch)	5'P-**CCTGAAGTTCATCTG**TGACAGGAAG**TAGATGAACTTTAGGGTCAGCTTGT** TGACAGGAAG**GCAAGCTGAC**
14	GFP-10 (27 bp)	5'P-**CCTGAAGTTCATCTGCA**TGACAGGAAG **TGCAGATGAACTTCAGGGTCAGCTTGC**TGACAGGAAG**GCAAGCTGAC**
15	GFP-10 (27 bp w/ mismatch)	5'P-**CCTGAAGTTCATCTGCA**TGACAGGAAG **TGTAGATGAATTTTAGGGTTAGCTTGT**TGACAGGAAG**GCAAGCTGAC**
16	GFP-10 (29 bp w/ mismatch)	5'P-**CCTGAAGTTCATCTGCACC**TGACAGGAAG **GGTGTAGATGAATTTTAGGGTTAGTTTGT**TGACAGGAAG**GCAAGCTGAC**
17	Luc-10 (21 bp)	**CTCTAGAGGATG**TGACAGGAAG**CATCCTCTAGAGGATAGAATG**TGACAGGAAG**CATTCTATC**
18	Luc-10 (25 bp)	5'P-**CTCAGCGTAAGTGAT**TGACAGGAAG **ATCACTTACGCTGAGTACTTCGATT**TGACAGGAAG**AATCGAAGTA**
19	Luc-12/6C (25 bp)*	5'P-**GAGCACTTCTTCATC**TGATAGGAAGTT**GATGAAGAAGTGCTCGTCCT** **CGTCC**CCCCCC**GGACGAGGAC**
20	GFP-12/6C (25 bp)	5'P-**CCTGAAGTTCATCTG**TGATAGGAAGTT **CAGATGAACTTCAGGGTCAGCTTGC**CCCCCC**GCAAGCTGAC**

i) Complementary regions highlighted in bold.

RCT Optimization

Rolling circle transcription was optimized according to a central composited design screen (SAS JMP 11). Reactions were all made to have a final volume of 25 µL with varying volumes of DNA template (3 µM), NTPs (25 mM each), and T7 RNA polymerase (50 U/µL). Reactions were allowed to proceed for 24 h at 37 ºC, treated with DNase, then analyzed by Quant-IT Ribogreen® assay and agarose gel electrophoresis (Supplementary Figure 1) to determine yield and the ratio of long/short product. Model selection was carried out using stepwise least squares regression with k-folds cross-validation (k = 5). The optimal models for predicting RNA yield and long/short RNA are shown in Supplementary Table 2.

Table S2. CCD Sreen for RCT Optimization from Template 6.

Pattern[a]	Vol. Template (µL)	Vol. Enzyme (µL)	Vol NTP (µL)	RNA Yield (µg/µL)	Long/Short RNA
+++	16	4	2	0.68	1.98
−++	4	4	2	0.06	0.01
+−+	16	0.5	2	0.09	0.00
−−+	4	0.5	2	0.01	0.00
−+−	4	4	0.5	0.18	1.20
−−−	4	0.5	0.5	0.02	0.00
0	10	2.25	1.25	0.35	2.47
00a	10	2.25	0.5	0.10	0.19
00A	10	2.25	2	0.22	1.05
A00	16	2.25	1.25	0.48	3.08
0a0	10	0.5	1.25	0.05	0.00
++−	16	4	0.5	0.27	1.46
+−−	16	0.5	0.5	0.06	0.00
0	10	2.25	1.25	0.32	3.02
0A0	10	4	1.25	0.69	3.05
a00	4	2.25	1.25	0.17	1.72

a) Patterns indicate relative amounts of different components used in the screen (0 = center point; a/- = lower point; A/+ = higher point).

Table S3. Fitted Parameters for Linear Models Predicting RNA Yield and Long/Short RNA

Y-Parameter	Term	Estimate	Std Error	t Ratio	Prob>|t|
RNA Yield	Intercept	0.3431243	0.054021	6.35	<.0001
RNA Yield	[Template](4,16)	0.1138413	0.041844	2.72	**0.0199**
RNA Yield	[Enzyme](0.5,4)	0.1650017	0.041844	3.94	**0.0023**
RNA Yield	[NTP](0.5,2)	0.0421143	0.041844	1.01	0.3358
RNA Yield	[NTP]*[NTP]	-0.174741	0.068332	-2.56	**0.0266**
Long/Short	Intercept	2.3876419	0.301311	7.92	<.0001
Long/Short	[Template](4,16)	0.3592858	0.210678	1.71	0.1265
Long/Short	[Enzyme](0.5,4)	0.7685621	0.210678	3.65	**0.0065**
Long/Short	[NTP](0.5,2)	0.0184949	0.210678	0.09	0.9322
Long/Short	[Template]*[Enzyme]	0.2794688	0.235546	1.19	0.2695
Long/Short	[Template]*[NTP]	0.2144736	0.235546	0.91	0.3891
Long/Short	[Enzyme]*[Enzyme]	-0.498333	0.388991	-1.28	0.236
Long/Short	[NTP]*[NTP]	-1.400933	0.388991	-3.6	**0.007**

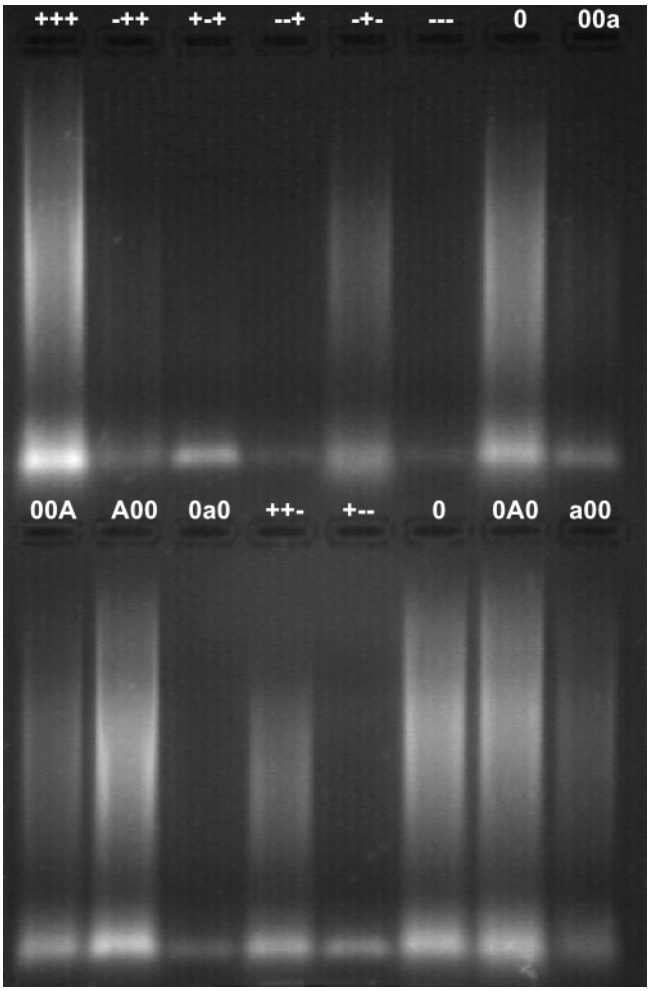

Figure S1. Agarose gel electrophoresis (1.5%, TBE) of reaction products from CCD screen described in Table S2.

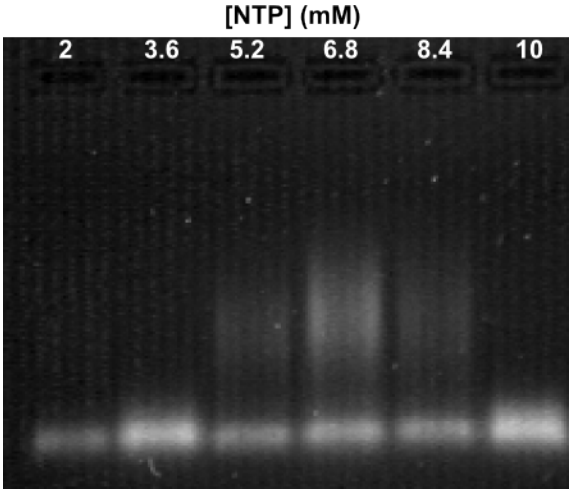

Figure S2. Agarose gel electrophoresis (1.5%, TBE) of follow-up experiment looking at effect of [NTP] on RCT.

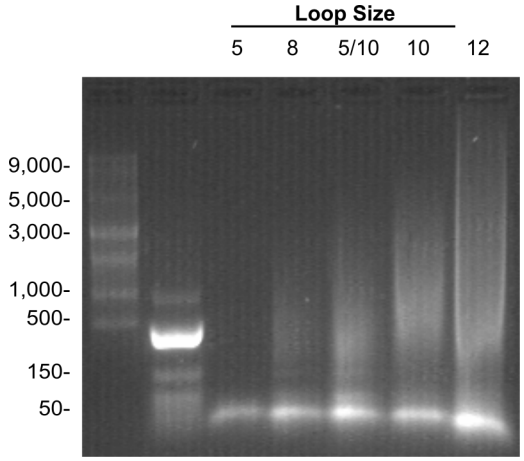

Figure S3. Agarose gel electrophoresis (1.5% TBE) of crude reaction products from templates with different loop sizes (from templates 2 ,4 , 5, 6, and 11).

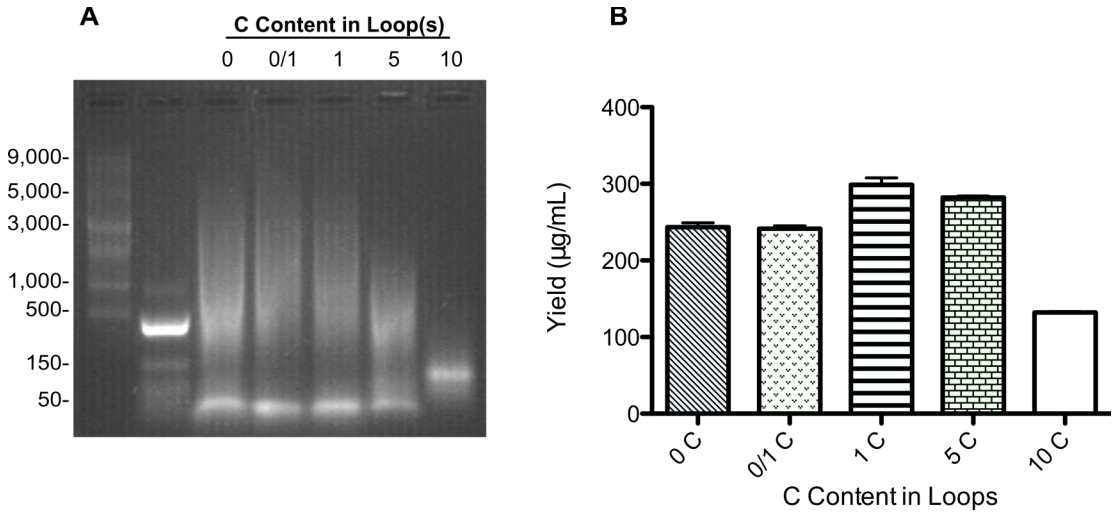

Figure S4. Influence of C content in dumbbell template loops on RCT. (A) Agarose gel electrophoresis (1.5%, TBE) of crude RCT reaction products from templates with 10 base loops, but different loop sequences (from templates 6-10). (B) RCT reaction yields measured by Quant-IT Ribogreen® (mean+s.e.m. for 3 reactions).

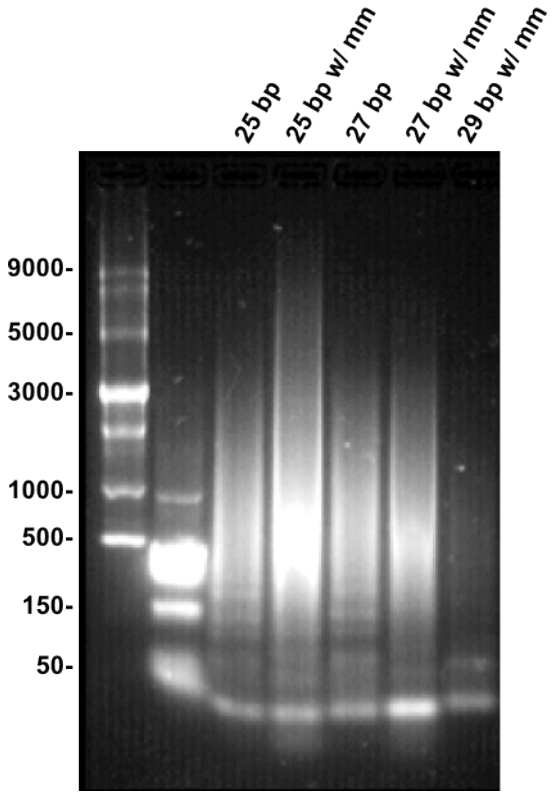

Figure S5. Agarose gel electrophoresis (1.5%, TBE) of RCT products from dumbbell templates with different stems. The templates used were #'s 9-13 (see Table S1).

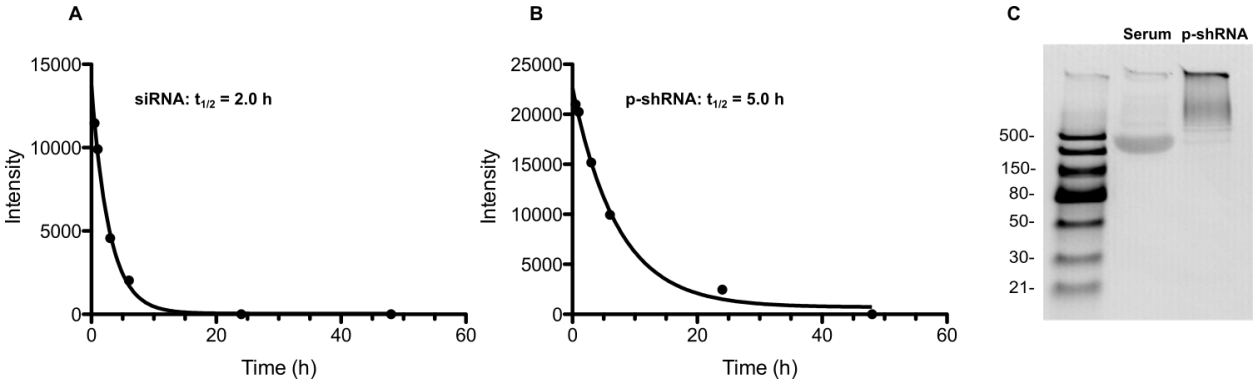

Figure S6. Degradation kinetics of siRNA (A) and csiRNA (B) in 50% human serum. Intensity corresponds to the 21 bp band intensity quantified with Image J from the gels shown in Figure 2D-E. (C) Serum only control lane with dsRNA ladder and untreated p-shRNA for reference.

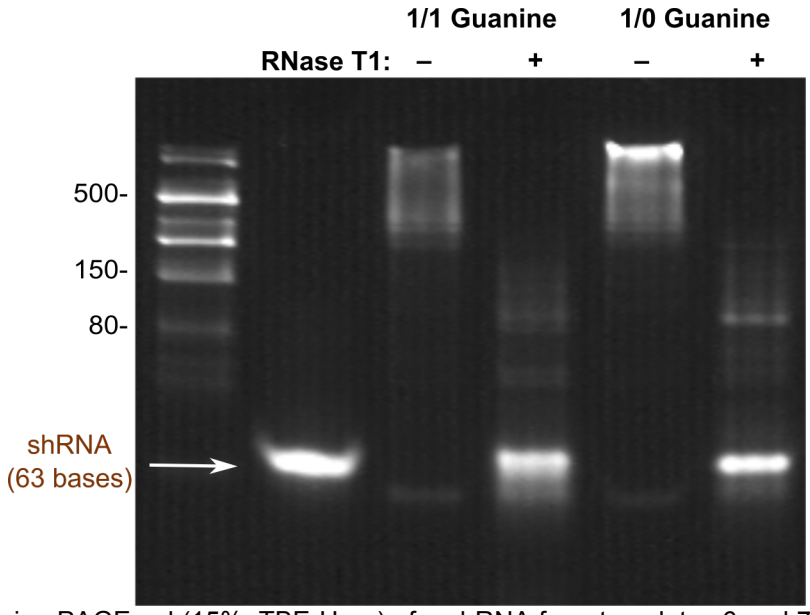

Figure S7. Denaturing PAGE gel (15%, TBE-Urea) of p-shRNA from templates 6 and 7, with and without RNase T1 treatment.

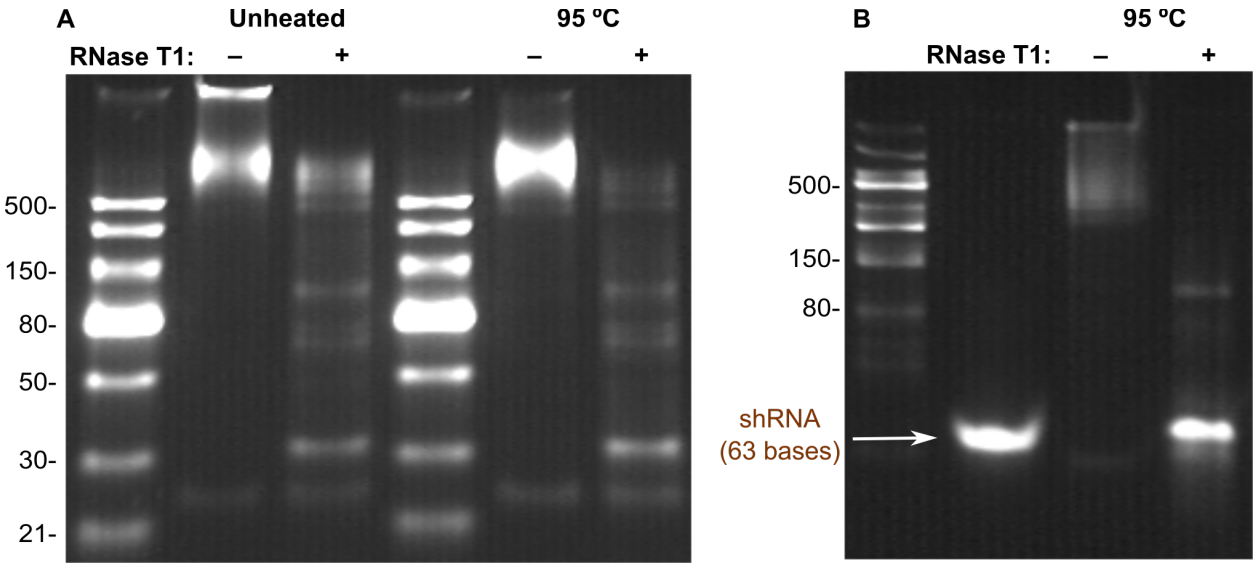

Figure S8. RNase T1 treatment of p-shRNA (from template 7) after heating to 95 ºC. (A) Native PAGE (15% TBE) and (B) denaturing PAGE (15% TBE-Urea).

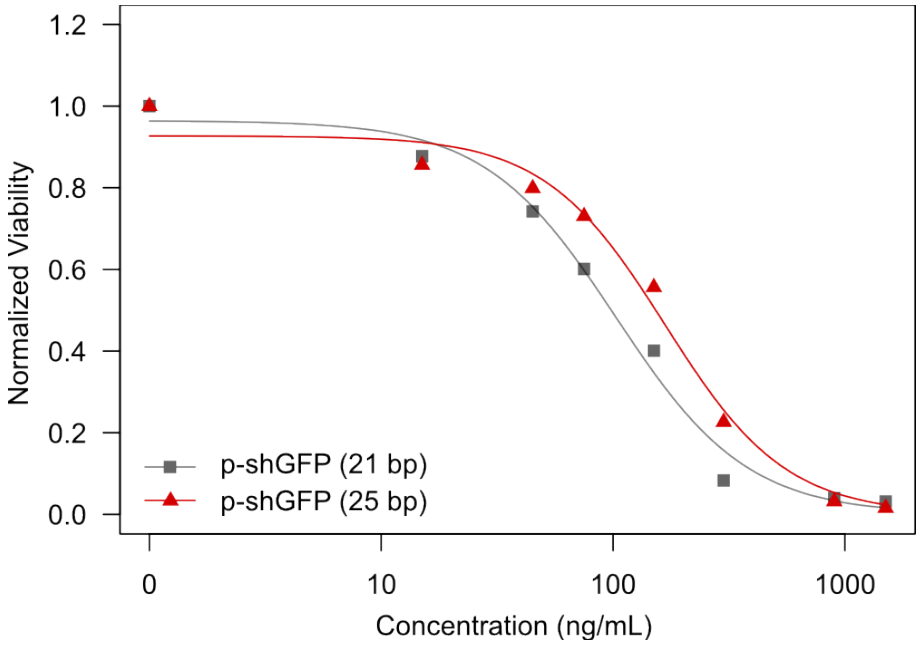

Figure S9. Cell viability curves for SKOV3 cells treated with 21 bp (from template 6) and 25 bp p-shRNA (from template 9) delivered with Lipofectamine 2000.

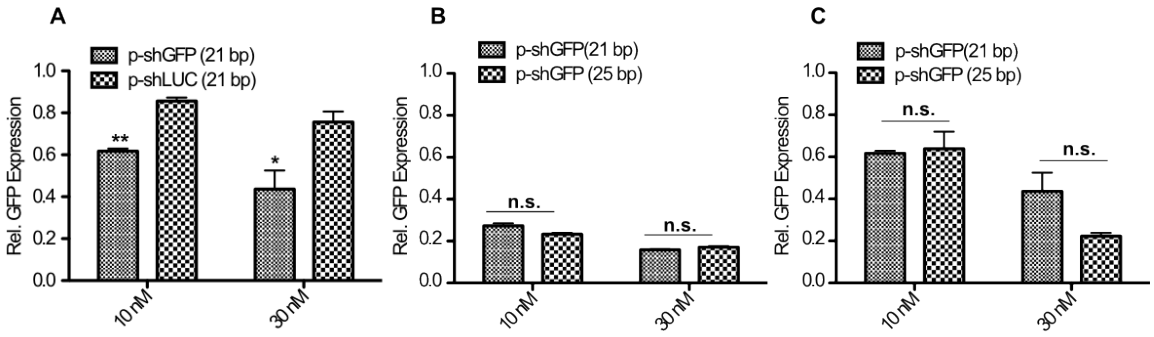

Figure S10. GFP knockdown in HeLa cells measured by flow cytometry (mean fluorescence). (A) GFP silencing by p-shRNA delivered with Lipofectamine 2000. (B-C) Comparison of silencing by 21 bp (from template 6) and 25 bp p-shRNA (from template 12), delivered with TransIT-X2 (B) or Lipofectamine 2000 (C). Samples were all normalized to the mean fluorescence of untreated cells and represent the mean of three biological replicates ± s.e.m. P<0.05 (*), P<0.01 (**), P<0.001 (***)

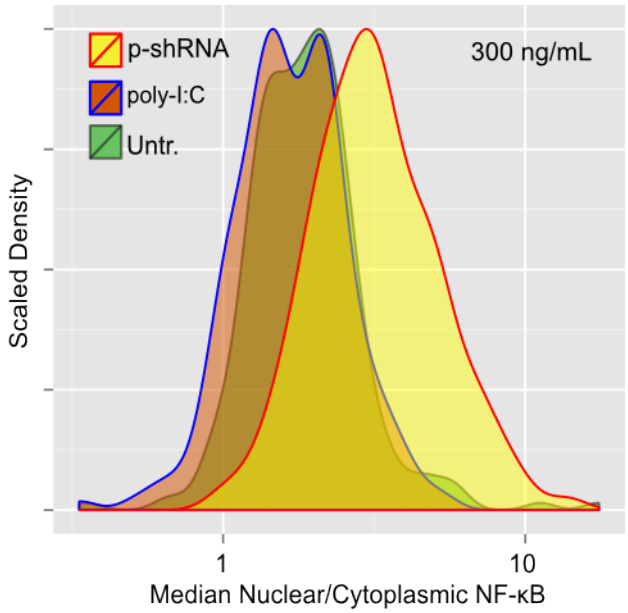

Figure S11. Nuclear localization of NF-κB was quantified using Cell Profiler by taking the ratio of median NF-κB fluorescence in the nucleus divided by median NF-κB fluorescence in the cytoplasm for untreated cells or cells treated with 150 ng/mL RNA/Lipofectamine complexes.

Supplemental Discussion

When we attempted to refold p-shRNA derived from template 7, this led to a substantial increase in the relative amount of single hairpins produced with RNase T1 treatment. Two possible scenarios are shown below, corresponding to initiation at the different loops:

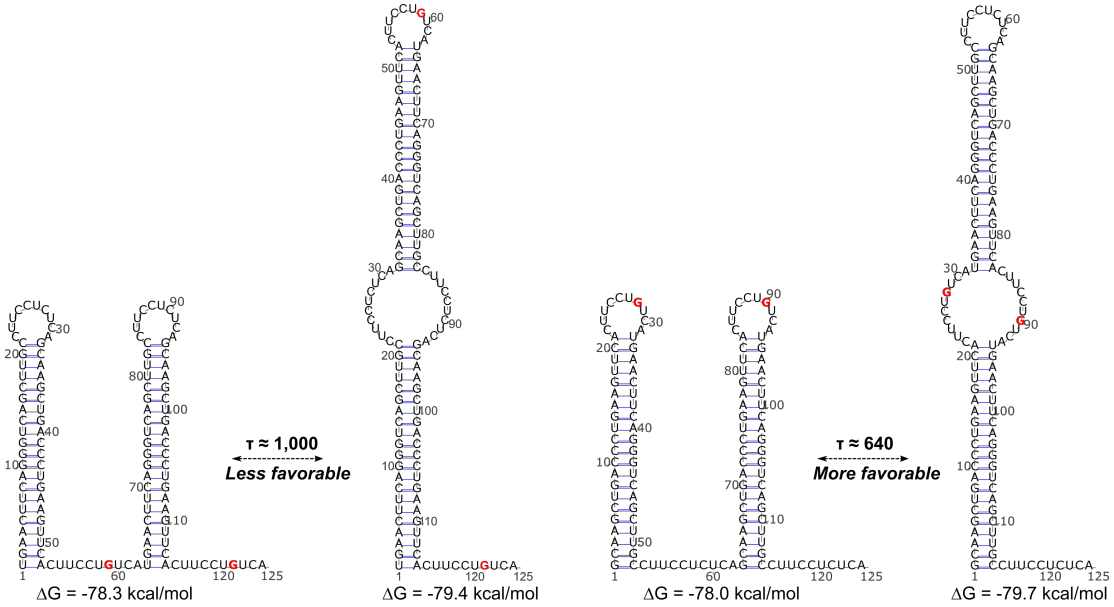

According to the CoFold folding predictions, the transition from a single hairpin to double hairpin structure is more kinetically favorable for the p-shRNA with Gs in the hairpin loops vs. p-shRNA with Gs in the linker region (lower value of τ where back-folded structure becomes favored). We therefore propose a scenario where the major products after thermal refolding are those on the far left and far right of the above diagram, which are predicted to give a product distribution similar to what we observed experimentally (i.e., mostly single hairpins with some larger fragments).

We also point out that two sets of energy parameters are available to model folding with CoFold: Turner-1999 (T) and Andrenescu-2007 (A). When using the A-parameters in place of the T-parameters, additional base pairing in linker regions is predicted for p-shRNA derived from template 7:

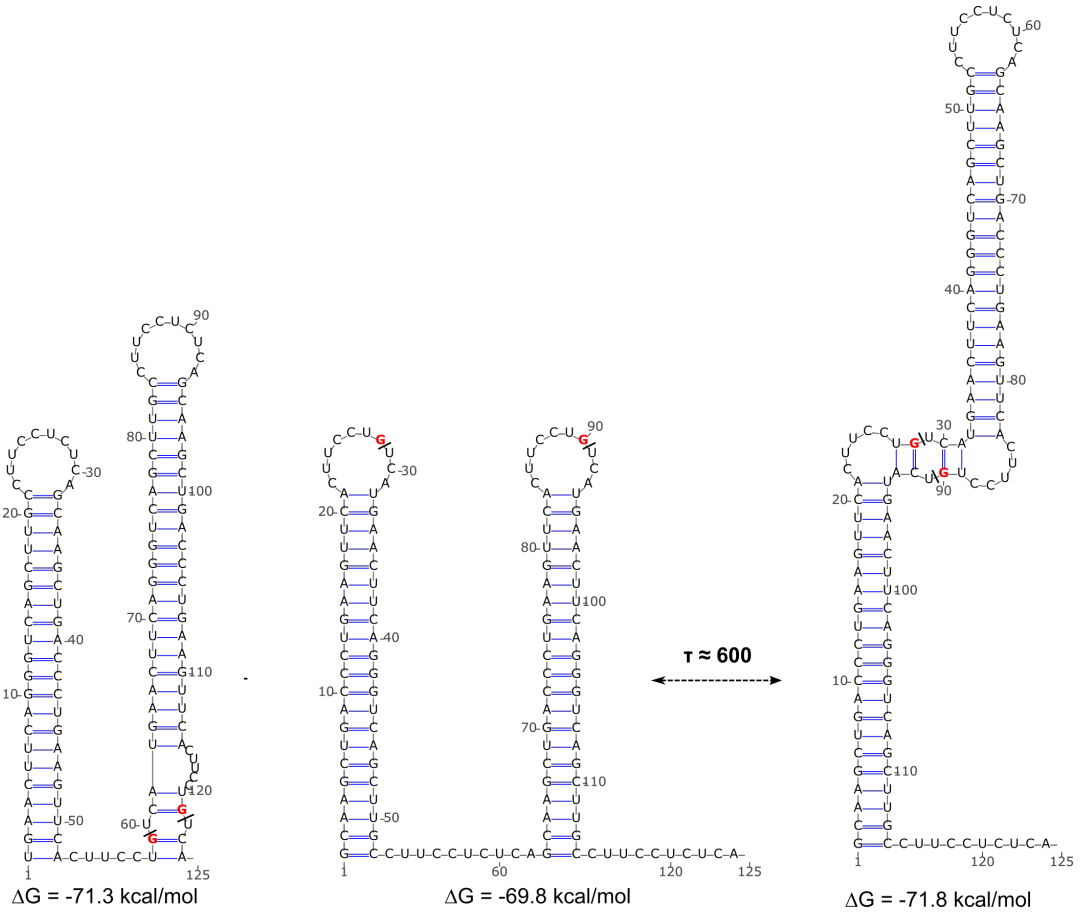

ΔG = -71.3 kcal/mol ΔG = -69.8 kcal/mol ΔG = -71.8 kcal/mol

With these additional base pairs, the structure with Gs at the bottom is further stabilized relative to the structure with Gs on top, and refolding to a more back-folded structure becomes even less kinetically favored for the structure on the left. On the other hand, the transition from the structure with Gs on top to the double-hairpin structure is now slightly more favorable, due to the new base pairs introduced upon refolding. We note here that these extra base pairs involve the RNase T1 cleavage sites, which we know from experiments must be labile. However, in other experiments (unpublished results) we observed that base-paired Gs adjacent to 3' single-stranded regions were still cleaved by RNase T1; as this would be the case in the above structures, they could still be consistent with our observations.